Pergamon

Int. J. Heat Mass Transfer. Vol. 39, No. 11, pp. 2333–2348, 1996
Copyright © 1996 Elsevier Science Ltd
Printed in Great Britain. All rights reserved
0017-9310/96 $15.00 + 0.00

0017-9310(95)00310-X

Natural convection for the melting of ice in porous media in a rectangular enclosure

WEN-JENG CHANG and DONG-FANG YANG

Graduate School of Mechanical Engineering, Feng Chia University, Taichung, Taiwan, Republic of China

(*Received* 6 *December* 1994)

Abstract—The transient behavior and heat transfer for the melting of ice in porous media within a rectangular enclosure is simulated by the numerical method SIMPLE C. The solid-liquid interface becomes irregular due to the presence of porous media. The mushy zone of the finite thickness is taken into consideration in this investigation. The entire flow field is modeled by the non-Darcy model which incorporates effects of convection, inertia and boundary friction. Based upon the numerical results, the non-linear factor due to temperature-dependent density of the molten liquid could be a significant contributor to temperature field, flow field, position of interface, and capacity of heat transfer. A temperature exists on the hot side where minimum heat transfer takes place. As the Darcy number gets larger, the heat transfer gets better, the rate of melting of ice goes faster, and the interface distorts more. As time goes on, heat transfer on the hot side worsens and that on the cold side gets better. Copyright © 1996 Elsevier Science Ltd.

INTRODUCTION

Solid/liquid phase change in porous media occurs widely in natural phenomena and industrial application, such as melting of soils, artificial freezing of ground for mining and construction purposes, freezing of soil around the heat exchanger coils of a ground based pump, thermal energy storage, freeze treatment of sewage, preparation of a semi-conductor, casting and welding of a manufacturing process, and so on. Therefore a better understanding about this phenomenon is necessary.

Early research in heat transfer in porous media with a phase change of fluid was dedicated to evaporation or condensation [1, 2]. Besides, the assumption was widely made, that heat transfer is governed by conduction only. Kazmierczak and Poulikakos [3], using simple boundary layer analysis, investigated natural convection in the melting liquid phase from a flat plate embedded in a porous medium and concluded that the convection of a liquid being molten played an important role.

When dealing with flow passing through porous media, early researchers assumed the applicability of Darcy law mostly for convenience, such as Kazmierczak and Poulikakos [3] and Zhang [4]. However, Darcy law is only applicable to low porosity and low speed fluid flow, since inertia and viscous effects are neglected herein. Some later researchers made further steps in analysis, such as Chen and Ho [5] by adding an inertia term; Tong and Subramanian [6] by adding a viscous term satisfying the no-slip condition; and Vafai and Tien [7] by adding boundary and inertia effects. Hence, non-Darcy law was developed which incorporates convection, inertia, boundary friction, thermal dispersion, and wall channelling effects for the appropriate description of fluid flow in a porous media. Related literature applying non-Darcy law for natural convection to a rectangular enclosure model where porous media and flow exist was partly accomplished by Beckermann *et al.* [8]. Later on, Beckermann and Viskanta [9] developed a general model for solid/liquid change with natural convection in the melting region of a porous media by using the non-Darcy law.

From the equation for density and temperature variation, it is found that the natural convection of water in low temperature is different from general fluid flow. This is due to the existing non-linear relationship between density and temperature in cold water and the fact that the maximum water density occurs at about 4°C under atmospheric pressure. Therefore, the linear Boussinesq equation employed in most of the literature regarding cold water is not applicable in the investigation of natural convection of cold water. In 1977, Gebhart and Mollendorf [10] formulated an adequate non-linear density-temperature relationship for water at a low temperature. Such an equation was used by Zhang [4], Lin and Nansteel [11], and so on. For steady state cold water which covers maximum density, Lin and Nansteel's [11] investigation for flow structure, temperature distribution, and heat transfer capacity, showed two eddies of equivalent strength and in an opposite sense would occur if a maximum density temperature line appeared in the geometry center of a rectangular enclosure.

As for the thickness of solid/liquid interface, general works concerning heat transfer of solid/liquid phase change would mostly assume zero thickness, e.g. Zhang [4]. But with the presence of porous media,

NOMENCLATURE

B	residual mass
c	specific heat [J kg^{-1} K^{-1}]
C	inertia coefficient, $1.75 \cdot \delta^{-3/2}/\sqrt{175}$
d_m	mean particle size [m]
Da	Darcy number, $K(\varepsilon)\ L^{-2}$
g	gravitational acceleration [m s^{-2}]
Δh	latent heat of fusion [J kg^{-1}]
H	height of cavity [m]
k_{eff}	effective thermal conductivity [W m^{-1} K^{-1}]
K	permeability $d_m\delta^3/175(1-\delta)^2$ [m^2]
KR	thermal conductivity ratio, k_{eff}/k_l
L	length of cavity [m]
LH	aspect ratio, H/L
Nu	local Nusselt number
$\overline{Nu}$	average Nusselt number
p	pressure [N m^{-2}]
P	dimensionless pressure, $pL^2/\rho_l\nu_l\alpha_l$
Pr	Prandtl number, ν_l/α_l
q	1.894816
R	maximum density parameter, $(T_m-T_c)/(T_h-T_c)$
Ra	modified Raleigh number, $\rho_{lm}g\lambda L^3(T_h-T_c)^q/\rho_l\nu_l\alpha_l$
Ste	Stefan number, $c_l(T_h-T_c)/\Delta h_{sl}$
t	time[s]
T	temperature [K] or [°C]
T_f	fusion temperature [°C]
T_m	maximum density temperature, 4.029325°C
u	x-direction velocity [m s^{-1}]
U	dimensionless x-direction velocity, uL/α_l
v	y-direction velocity [m s^{-1}]
V	dimensionless y-direction velocity, vL/α_l; volume [m^3]
x	horizontal coordinate [m]
X	dimensionless horizontal coordinate, x/L
y	vertical coordinate [m]
Y	dimensionless vertical coordinate, y/L.

Greek symbols

α	thermal diffusivity [m^2 s^{-1}]
γ	fraction liquid in fluid
δ	fraction liquid in volume element
ε	porosity
θ	dimensionless temperature, $(T-T_c)/(T_h-T_c)$
θ_f	dimensionless fusion temperature, $(T_f-T_c)/(T_h-T_c)$
κ	permeability ratio, $K(\varepsilon)/K(\delta)$
λ	9.297173×10^{-6} °C^{-q}
μ	dynamic viscosity [N s m^{-2}]
ν	kinematic viscosity [m^2 s^{-1}]
ρ	density [kg m^{-3}]
ρ_{lm}	maximum density, 999.972 kg m^{-3}
ρc	mean thermal capacitance [J m^{-3} K^{-1}]
τ	dimensionless time, $t\alpha_l/L^2$
Φ	physical quantity
Ω	thermal capacitance ratio, $\overline{\rho c}/\rho_l c_l$.

Subscripts

c	cold side
f	fusion
h	hot side
l	liquid
0	initial
p	porous medium
s	solid.

the interface in the coexisting solid and liquid region becomes an irregular curve owing to the interaction between liquid water and the porous media. If we persist in the assumption of zero thickness, we will miss out such physical phenomenon. From Beckermann and Viskanta's [9] study with glass marbles as the porous media and gallium as the fluid, they find, with the presence of porous media, the generation of dendrites near the fusion temperature of gallium, which makes the solid/liquid interface extremely irregular. Finite thickness of the coexisting solid and liquid zone, that is, the solid/liquid region of finite thickness, is hence considered for within limited temperature range near fusion temperature.

Reviewing past researches, the topic of the solid/liquid phase change heat transfer has not yet been thoroughly studied. Especially, no work has been done with simultaneous considerations for the non-linear density-temperature relationship, mushy zone, and transient natural convection applying non-Darcy effect for the melting of ice in porous media within a rectangular enclosure, therefore, we decided to contribute to the study of the transient behavior of the melting of ice in porous media.

THEORETICAL ANALYSIS

Figure 1 shows us the physical model and coordinate system for a rectangular enclosure in porous media which contains pure solid ice inside before we start the numerical operation. x represents the horizontal coordinate and y the vertical coordinate. H and L stand for, respectively, height and width of the rectangular enclosure whose top and low surface are both maintained adiabatic. At $t = 0$, the temperature

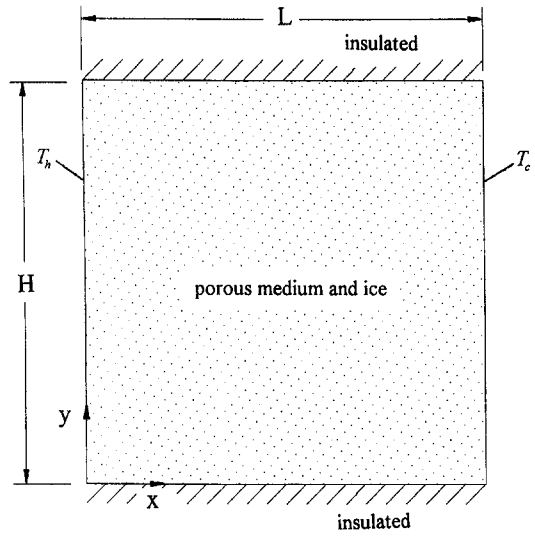

Fig. 1. The physical model and coordinate system.

on the left hand side is suddenly set to some high value and that on the right still remains at its initial value.

For better analysis, some assumptions have been made:

(1) a two dimensional flow field and ice zone;

(2) the phase change material and porous media reach local thermal equilibrium;

(3) constant porosity and iso-orientation of porous media;

(4) the porous media and ice are immovable (i.e. $u_p = u_s = 0$);

(5) assumptions for laminar flow, insignificant viscous heat dissipation and insignificant radiative heat transfer;

(6) density change is neglected (i.e. $\rho_l = \rho_s = \rho_f$) where phase change occurs;

(7) the physical properties of the fluid flow are all assumed constant except the non-linear density-temperature equation in the buoyant term.

Concerning the density-temperature equation, we will follow the one derived by Gebhart and Mollendorf [10]

$$\rho = \rho_{lm}(1 - \lambda|T - T_m|^q). \tag{1}$$

Among them, $\rho_{lm} = 999.972\ \mathrm{kg\,m^{-3}}$ (maximum density of water), $\lambda = 9.297173 \times 10^{-6}\ ^\circ\mathrm{C}^{-q}$, $T_m = 4.029325^\circ\mathrm{C}$ (maximum density temperature of water), and $q = 1.894816$.

Then, applying the theorem of conservation and introducing the dimensionless parameters as below

$$X = \frac{x}{L} \quad Y = \frac{y}{L} \quad U = \frac{uL}{\alpha_l}$$

$$V = \frac{vL}{\alpha_l} \quad P = \frac{pL^2}{\rho_l v_l \alpha_l} \quad \tau = \frac{t\alpha_l}{L^2}$$

$$\theta = \frac{T - T_C}{T_h - T_C} \quad \theta_f = \frac{T_f - T_C}{T_h - T_C} \quad \theta_0 = \frac{T_0 - T_C}{T_h - T_C} \quad Pr = \frac{v_l}{\alpha_l}$$

$$Da = \frac{K(\varepsilon)}{L^2} \quad KR = \frac{k_{eff}}{k_l}$$

$$Ra = \frac{\rho_{lm} g \lambda L^3 (T_h - T_C)^q}{\rho_l v_l \alpha_l} \quad R = \frac{T_m - T_C}{T_h - T_C}$$

$$Ste = \frac{c_l(T_h - T_C)}{\Delta h_{sl}} \quad \Omega = \frac{\overline{\rho c}}{\rho_l c_l}$$

$$\kappa = \frac{K(\varepsilon)}{K(\delta)} \quad \delta = \varepsilon\gamma, \quad LH = \frac{H}{L}, \tag{2}$$

we obtain the following dimensionless governing equations:

continuity equation

$$\frac{\partial U}{\partial X} + \frac{\partial V}{\partial Y} = 0 \tag{3}$$

x-momentum equation

$$\frac{1}{\delta}\frac{\partial U}{\partial \tau} + \frac{1}{\delta^2}\left(U\frac{\partial U}{\partial X} + V\frac{\partial U}{\partial Y}\right) = -Pr\frac{\partial P}{\partial X} + \frac{Pr}{\delta}\left(\frac{\partial^2 U}{\partial X^2} + \frac{\partial^2 U}{\partial Y^2}\right) - \left[\frac{\kappa \cdot Pr}{Da} + \frac{C \cdot \kappa^{1/2}}{\sqrt{Da}}\sqrt{U^2 + V^2}\right]U \tag{4}$$

y-momentum equation

$$\frac{1}{\delta}\frac{\partial V}{\partial \tau} + \frac{1}{\delta^2}\left(U\frac{\partial V}{\partial X} + V\frac{\partial V}{\partial Y}\right) = -Pr\frac{\partial P}{\partial Y} + \frac{Pr}{\delta}\left(\frac{\partial^2 V}{\partial X^2} + \frac{\partial^2 V}{\partial Y^2}\right) - \left[\frac{\kappa \cdot Pr}{Da} + \frac{C \cdot \kappa^{1/2}}{\sqrt{Da}}\sqrt{U^2 + V^2}\right]V + Ra \cdot Pr \cdot [|\theta - R|^q - |\theta_f - R|^q] \tag{5}$$

and energy equation

$$\Omega\frac{\partial \theta}{\partial \tau} + U\frac{\partial \theta}{\partial X} + V\frac{\partial \theta}{\partial Y} = \nabla \cdot (KR\nabla T) - \frac{1}{Ste}\frac{\partial \delta}{\partial \tau}. \tag{6}$$

Since we will treat the entire field, the four equations from (3) to (6) each can be used to solve the ice region, the mushy or coexisting ice and water region, and the water region. Also, when calculating the physical properties, the following conditions will be implemented into equations (3)–(6) for solutions: $\gamma = 1$ and $\delta = \varepsilon$ for the interface between the water and mushy region as well as the water region; $0 < \gamma < 1$ and $0 < \delta < \varepsilon$ for the mushy region; $\gamma = 0$, $\delta = 0$ for the interface between the mushy and water region as well as for the ice region. Therefore, boundary conditions are only required for four sides of rectangular enclosure. The initial and boundary conditions for the dimensionless equations are as follows:

initial conditions (at $\tau = 0$)

$$\theta = \theta_0 = 0, \quad U = V = 0$$
$$\text{for } 0 \leqslant X \leqslant 1 \quad 0 \leqslant Y \leqslant LH \tag{7}$$

boundary conditions

$$\theta = 1 \quad U = V = 0 \quad \text{for } X = 0 \quad 0 \leqslant Y \leqslant LH$$
$$\theta = 0 \quad U = V = 0 \quad \text{for } X = 1 \quad 0 \leqslant Y \leqslant LH$$
$$\frac{\partial \theta}{\partial Y} = 0 \quad U = V = 0 \quad \text{for } Y = 0 \quad 0 \leqslant X \leqslant 1$$
$$\frac{\partial \theta}{\partial Y} = 0 \quad U = V = 0 \quad \text{for } Y = LH \quad 0 \leqslant X \leqslant 1. \tag{8}$$

The important parameter in convection problems, Nusselt number, indicates the capacity of heat transfer in dimensionless form. It can be defined as below:

dimensionless local Nusselt number, Nu;

$$Nu_h = -\left.\frac{\partial \theta}{\partial X}\right|_{X=0} \text{ at hot side;}$$
$$Nu_C = -\left.\frac{\partial \theta}{\partial X}\right|_{X=1} \text{ at cold side} \tag{9}$$

dimensionless average Nusselt number, $\overline{Nu}$;

$$\overline{Nu_h} = \frac{1}{LH}\int_0^{LH} Nu_h \, dY \quad \text{at the hot side;}$$
$$\overline{Nu_C} = \frac{1}{LH}\int_0^{LH} Nu_C \, dY \quad \text{at the cold side.} \tag{10}$$

NUMERICAL METHOD

The numerical method SIMPLE-C, incorporating the power-law scheme, developed by Patankar and Spalding [13] in 1972, and detailed by Patankar [14], is used. For quicker convergency, this method was modified by Van Doormaal and Raithby [12] in 1984.

The mushy zone is defined as the region with a space span of half of the diameter of the particle both to the left and right from the position where θ_f, the dimensionless fusion temperature, is located. The equations for the mushy zone will be used for the solutions. Points with temperature higher than that of the mushy zone will be considered located in the fluid flow region, where the fluid flow equations are applicable; likewise, points with temperature lower than that will be considered located in the ice region where equations for the ice regions are valid. If the values of U, V, P, θ calculated after iteration do not meet the convergency criteria when compared with those obtained from previous iteration, they will again be iterated until convergency. When convergency comes, the values obtained are then the solutions for that particular time. We repeat this operation with advancing time step until steady state is attained.

In spacing, we employ constant spacing for the entire rectangular space. Before we started the calculation, we first meshed the geometry in a constant spacing for test with grid points of 21×21, 33×33, 41×41, 66×33, 99×33, 99×41, 132×33. For an arbitrary two among the previous four spacings, at least one average Nusselt number difference on the hot side is above 5% when time is equal to 30, 90 and 240 min, respectively; and for the later three of spacings, all average Nusselt number differences on the hot side are below 5% when time is equal to 30, 90 and 240 min, respectively. Considering the accuracy of the solutions and efficient calculation, we hence select a constant spacing meshing of 99×33.

The line by line method is first used to transform the finite difference equations into three diagonal matrices and then the tridiagonal matrix algorithm (TDMA) will be applied for the solution. Alternative direction implicit procedures (ADI) are employed for iteration with the under-relaxation factor considered for sweep in four directions: upward, downward, forward and backward.

The convergency criteria for every time step is residual mass B is less than 10^{-5} and the residual values for U, V, θ are

$$R = \Sigma a_{nb}\Phi_{nb} + b - a_P\Phi_P < 10^{-4}$$

where Φ could be U, V or θ.

The convergency criteria for steady state is

$$|\overline{Nu_h} - \overline{Nu_C}| \leqslant 10^{-2},$$

where $\overline{Nu_h}$, $\overline{Nu_c}$ represent average Nusselt number for the hot and cold sides, respectively.

RESULTS AND DISCUSSION

The characteristic length L equals 6.5 cm and temperature on the cold side T_C is maintained at a constant of $-0.5°C$ in this paper. Our investigation is mainly to discover the influence on the flow field, temperature distribution, interface position, and heat transfer capacity with respect to maximum density parameter R, permeability k (i.e. Darcy number Da), and time variable t. We change the maximum density parameter, R, by adjusting the hot side temperature T_h. The correlation between the two is: as $T_h = 12°C$, $R = 0.36$; $T_h = 8°C$, $R = 0.53$; $T_h = 4°C$, $R = 1.01$. The change of T_h is also accompanied by a change of the modified Raleigh number Ra and Stefan number Ste. The value ranges of the dimensionless physical parameters are: Prandtl number $Pr = 11.8$; aspect ratio $LH = 1$; porosity $\varepsilon = 0.4$; Darcy number, Da, from 3×10^{-7} to 3×10^{-5}; modified Raleigh number, Ra; from 2.5×10^6 to 5×10^7; maximum density parameter, R; from 0.36 to 1.81; and Stefan number Ste; from 0.03 to 0.16.

Figures 2 to 4 show the influence to the flow field as a result of various hot side temperatures. As time increases, the region of flowing liquid water expands, i.e. an increase of liquid water from the melting of ice. The temperature difference between the hot and cold sides varies with respect to change of T_h with which the increase rate of the flowing liquid water region also varies as time goes on. The maximum and minimum rates occur when T_h equals 12 and 4°C, respectively.

Figure 5 explains the time-related change of the interface position, defined as the isothermal line of fusion temperature of ice for various temperatures on the heating side. It is shown that: the interface tends to move towards the cold side as time goes on, and to shift speeds of the upper and lower parts of the interface which vary with T_h. For instance, Fig. 5a and b illustrates the heating conditions for T_h equal to 12 and 10°C, respectively, which shows that the upper part shifts faster than the lower as a result of better fusion rate in the upper portion. This is attributed to the stronger and clockwise eddy on the left side which facilitates direct heat transfer from the hot side to the upper part of the interface. Figure 5c–f corresponding to T_h equal to 8, 6, 4 and 2°C, respectively, shows a greater shifting speed on the lower interface as a result of better fusion rate in the lower portion. This is because the fluid near the interface is influenced by a counterclockwise eddy accordingly.

The variations of local Nusselt numbers of the hot and cold sides at different times while T_h is equal to 12, 8 and 4°C are shown in Figs 6–8 respectively. It is found that as time increases, the local Nusselt number becomes smaller for the hot side and larger for the cold side. At $T_h = 12$°C, as indicated in Fig. 6, minimum heat transfer flux occurs at $Y = 1$ and maximum heat transfer occurs at $Y = 0$ on hot side. It is explained as follows: the density of the fluid near the hot side after being heated becomes smaller than the maximum density and then moves up and absorbs energy gradually. When reaching the top of the hot side, its temperature is therefore at its highest which causes a low temperature gradient and poor heat transfer flux therein. As the clockwise main eddy brings cooler fluid near the cold side to the bottom of the hot side, the temperature gradient, and hence the heat transfer flux increases. Likewise, the maximum heat transfer flux occurs at the top of the cold side and the bottom of the cold side becomes the minimum, which can be explained by the above influence from the clockwise main eddy. Figure 7 shows that the difference between the maximum and minimum heat transfer on the hot side is smaller than that for the case of $T_h = 12$°C in Fig. 6, which is mainly due to the fact that the cooler fluid from the cold side fails to reach the hot side as a result of two equivalent eddies generated when $T_h = 8$°C (Fig. 3). Figure 8 illustrates that the maximum heat transfer flux happens both on the top of the hot side and the bottom of the cold side while minimum heat transfer flux occurs at the bottom of the hot side and top of the cold side. The explanation for this is that the counterclockwise and cooler fluid flow from the cold side has direct contact with the top of the hot side, which enables greater temperature difference and thus better heat transfer on the top of the hot side; later once the cooler fluid flow becomes warmer and its density larger, it begins to flow down to below the hot side where the fluid temperature increases and heat transfer capacity decreases. The warm flow continues to flow to the bottom of the cold side and finally the temperature difference becomes bigger and hence the heat transfer is better.

The influence of the maximum density parameter R to flow field at 600 min is seen in Fig. 9. We find as $R = 0.36$, the clockwise eddy on the left is bigger than the counterclockwise one on the right; $R = 0.53$, both eddies are equivalent, however with a further increase of R, the counterclockwise eddy on the right becomes bigger. When R exceeds 1, the one on the left will vanish and only one counterclockwise eddy remains, which is due to the moving-down of the fluid of greater density near the hot side as a result of the fact that the maximum density isothermal line ($\theta = R$) shifts out of the flow region.

The influence of the maximum density parameter R to the interface position and fusion rate for $t = 30$, 120 and 360 min is illustrated in Fig. 10. Figure 10a shows the following scenario: as R gets smaller and less than 0.53, the interface tends to distort toward the cold side as the vertical coordinate increases, which means fusion gets faster with respect to the increase of the vertical coordinate, because the bigger main clockwise eddy transfers the heat of the warm flow from the hot side to the upper part of the interface. However, as R becomes larger and greater than 0.53, the interface tends to distort toward the cold side as the vertical coordinate decreases, which represents fusion going faster with respect to the decrease of the vertical coordinate because the bigger counterclockwise eddy transfers the heat of warm flow from the hot side to the lower part of the interface. Figure 10a and b both share the same tendency. More is revealed in Fig. 10c as the Darcy number equals 3×10^{-7}, the interface remains nearly vertical regardless of the value of R, which signifies that under this permeability the convection effect is insignificant, i.e. heat transfer is only dominated by heat conduction.

The influence of the hot side temperature T_h to average the Nusselt number on the hot side at $t = 975$ min is shown in Fig. 11. $\overline{Nu}$ does not always increase with respect to increase of T_h, i.e. a decrease of R. There exists a hot side temperature of 8°C for a minimum heat transfer, which is because under this kind of heating condition two equivalent eddies are generated in the flow field, and in opposite sense, results in indirect heat transfer and thus higher average temperature and poorer heat transfer for the left eddy. As $2°C \leqslant T_h \leqslant 8°C$, there exists a local maximum heat transfer capacity for $\overline{Nu}$ at 4°C. This happens due to the formation of only one counterclockwise eddy at

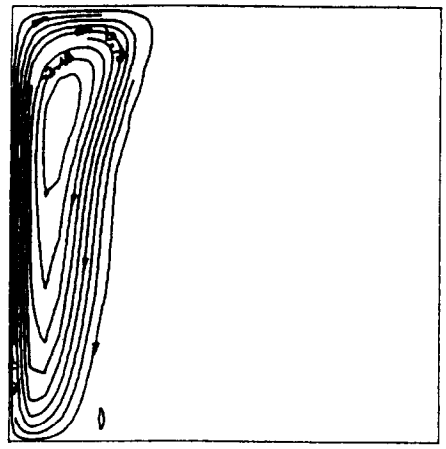

(a) t=30min

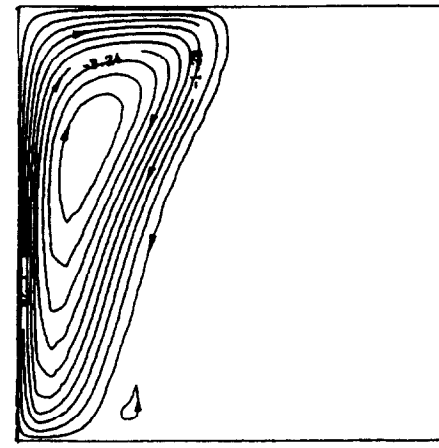

(b) t=60min

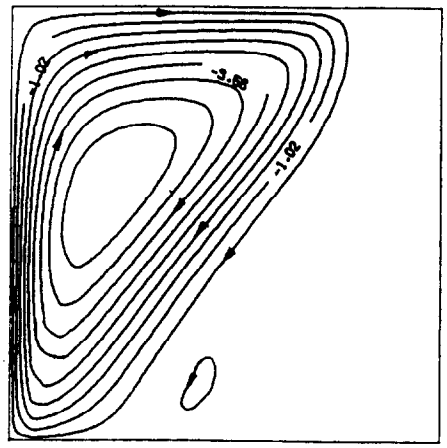

(c) t=120min

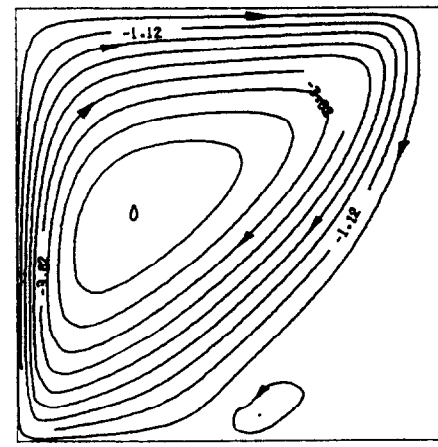

(d) t=240min

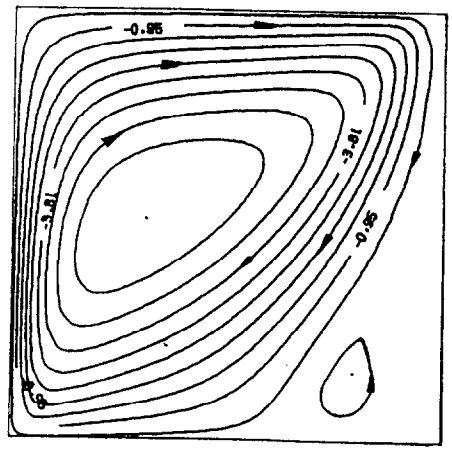

(e) t=360min

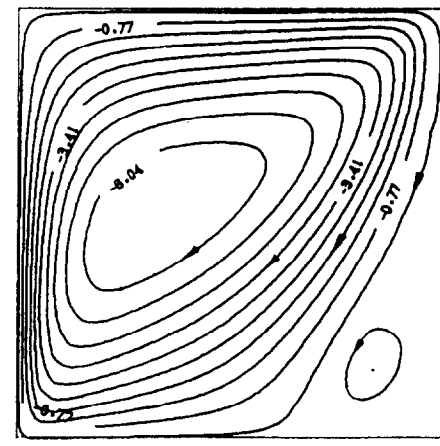

(f) t=480min

Fig. 2. The contours for time dependent streamlines for $R = 0.36$ ($Ra = 5 \times 10^7$, $Ste = 0.16$, $Da = 6 \times 10^{-6}$).

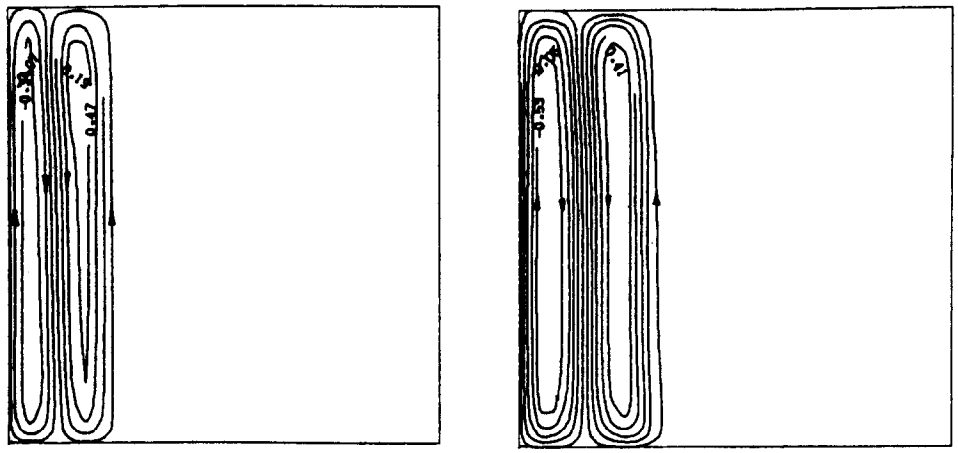

(a) t=30min (b) t=60min

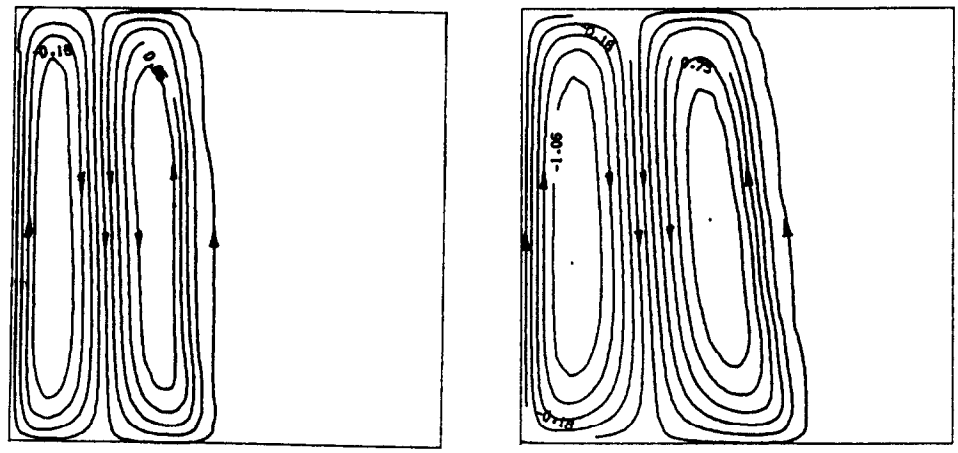

(c) t=120min (d) t=240min

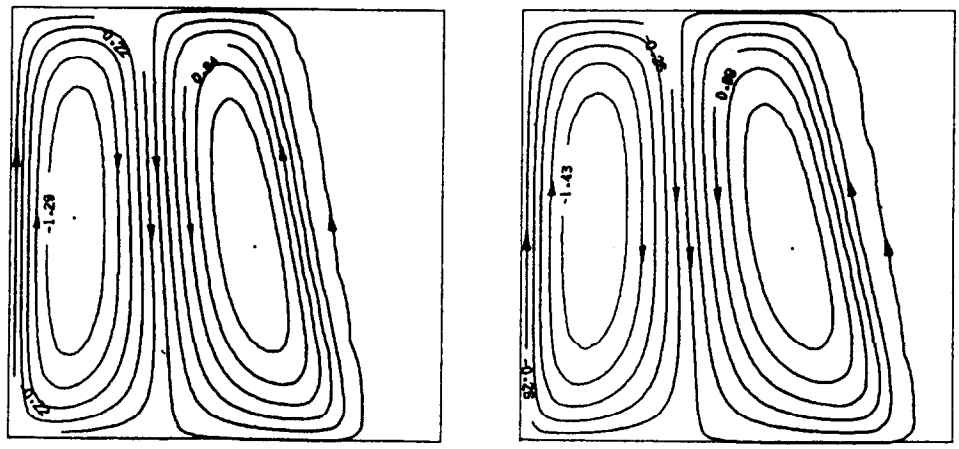

(e) t=360min (f) t=480min

Fig. 3. The contours for time dependent streamlines for $R = 0.53$ ($Ra = 2.5 \times 10^7$, $Ste = 0.11$, $Da = 6 \times 10^{-6}$).

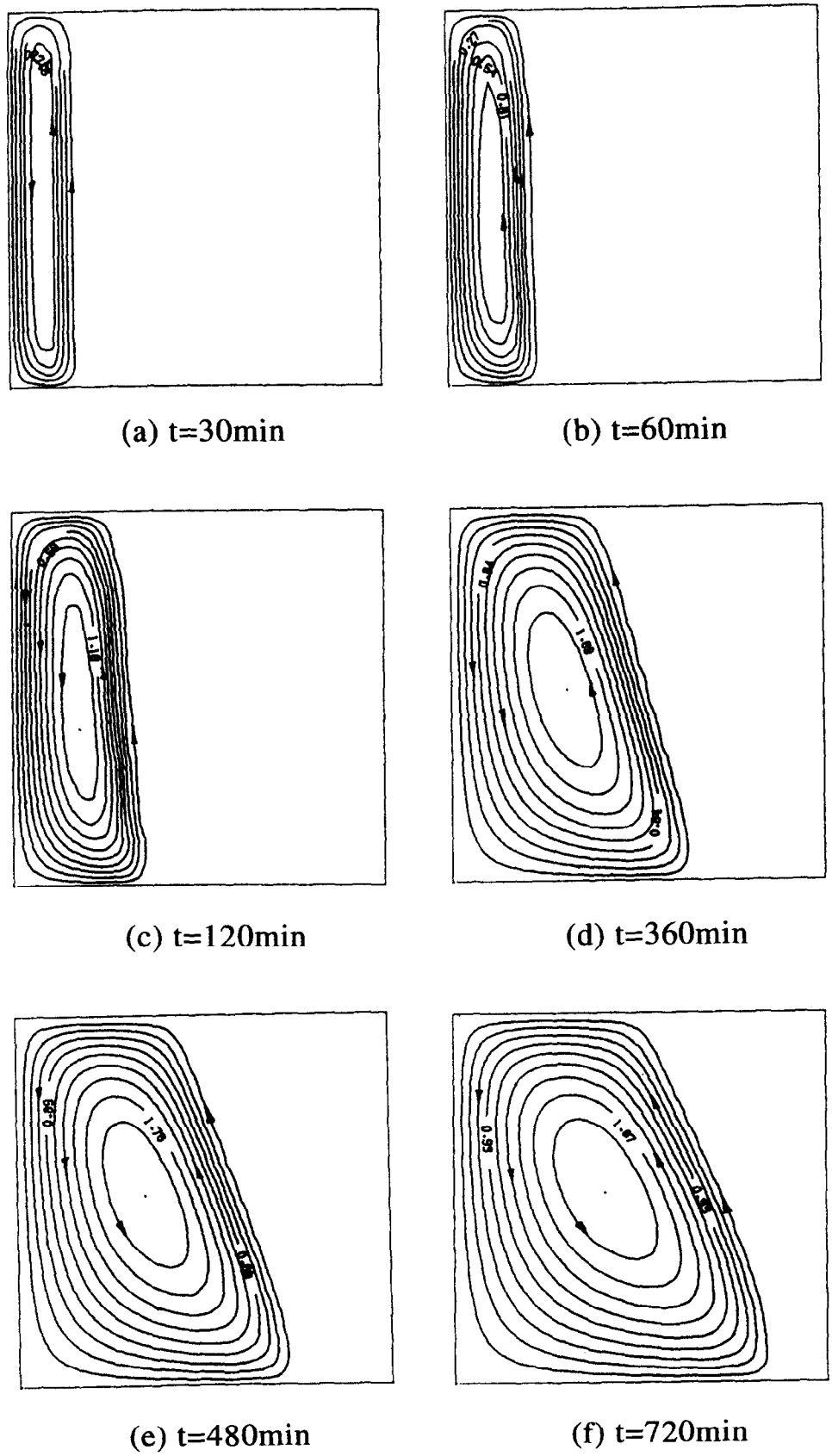

Fig. 4. The contours for time dependent streamlines for $R = 1.01$ ($Ra = 7.5 \times 10^6$, $Ste = 0.06$, $Da = 6 \times 10^{-6}$).

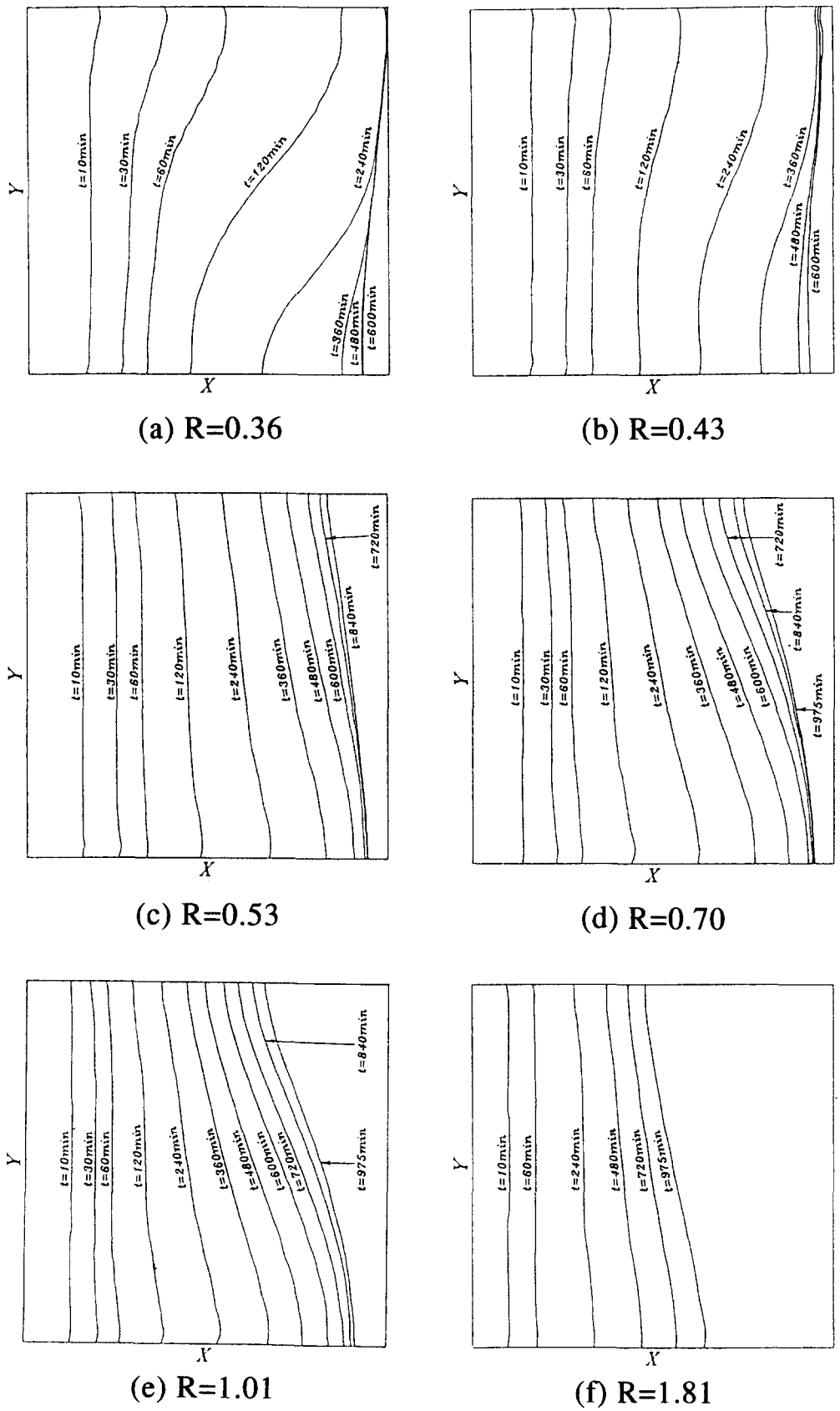

Fig. 5. The variations of the interface positions at various values of time ($Da = 6 \times 10^{-6}$).

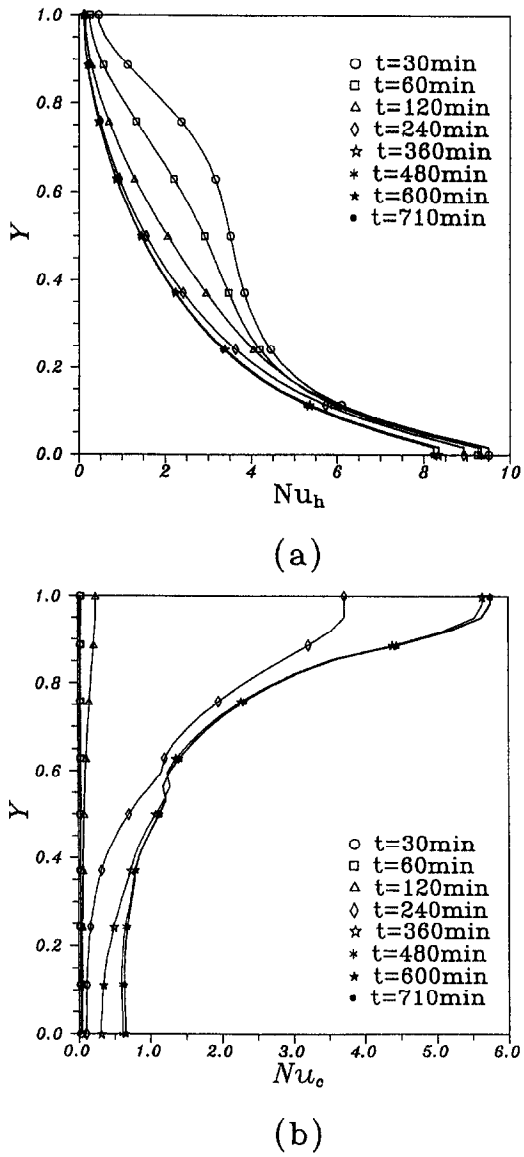

Fig. 6. The variations of the local Nusselt number at eight different values of time for $R = 0.36$, (a) hot side, (b) cold side ($Da = 6 \times 10^{-6}$).

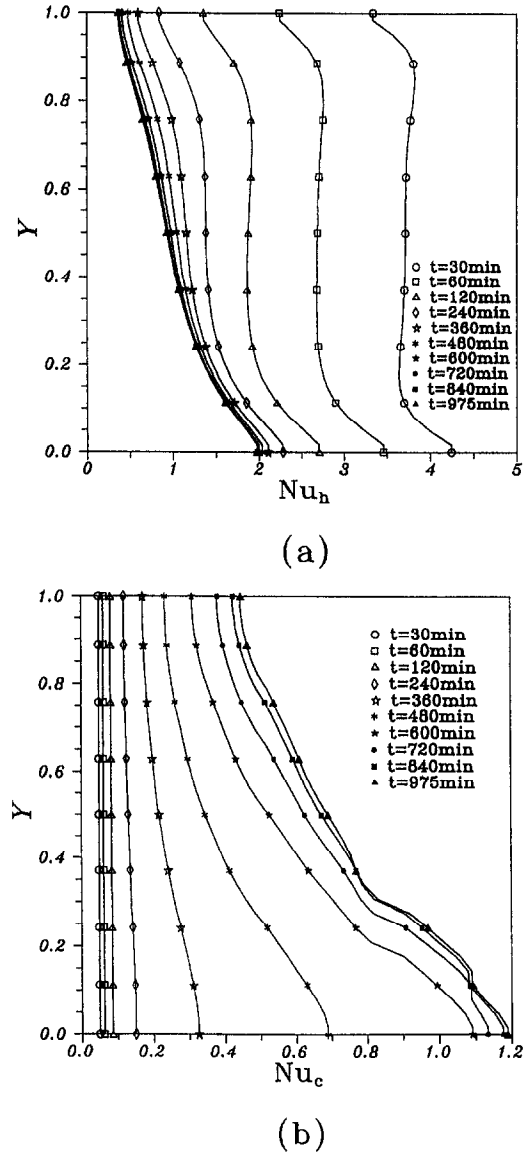

Fig. 7. The variations of the local Nusselt number at eight different values of time for $R = 0.53$, (a) hot side, (b) cold side ($Da = 6 \times 10^{-6}$).

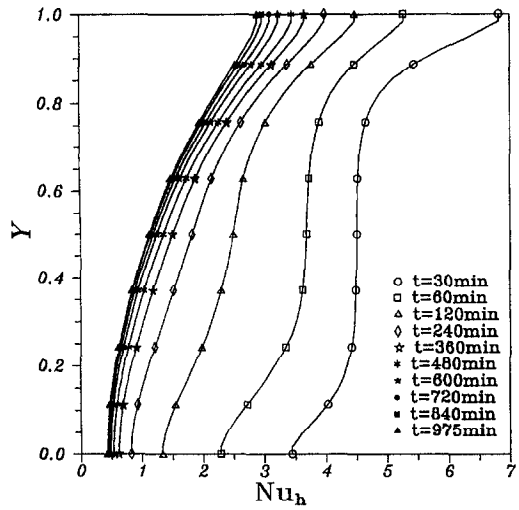

(a)

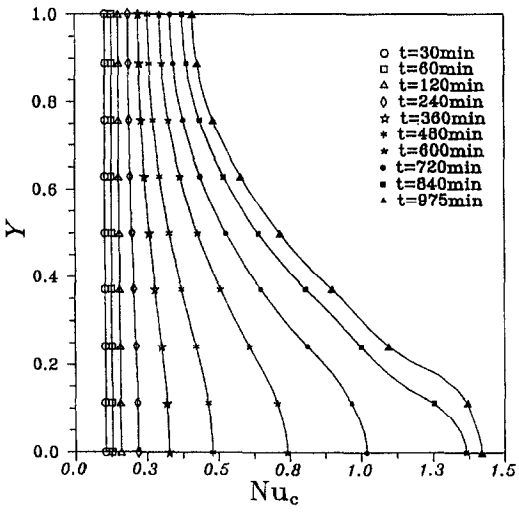

(b)

Fig. 8. The variations of the local Nusselt number at eight different values of time for $R = 1.01$, (a) hot side, (b) cold side ($Da = 6 \times 10^{-6}$).

4°C which produces a better convective effect than at any other T_h. As $T_h > 8$°C, Nu increases abruptly due to the increase of the hot side temperature and hence, better convection occurs.

The Darcy number is an index of permeability, the higher the Darcy number is, the better the permeability is. When the fluid can more easily flow through a porous media, a better convection could be expected. As shown in Fig. 12 with two equivalent eddies of opposite senses, these two tend to move toward the upper part of the geometry center and thus isothermal lines concentrate more here when the Darcy number becomes bigger. From Fig. 10, we also understand the influence of the Darcy number Da to the interface position, and fusion rate at $t = 30$, 120 and 360 min. As the Darcy number increases, the interface distorts more and the fusion rate becomes greater. When $R = 0.36$ (solid line), the fusion rate in the upper part of the interface is always larger than that in the lower, due to heat transfer to the upper resulting from the presence of a stronger clockwise eddy in the left; for $R = 0.53$ (long dotted line) and $t = 30$ min, the interface changes little with regard to the Darcy number as a result of less fluid in the flow field and insignificant flow speed. At $t = 360$ min, the interface bends more as the Darcy number gets bigger, which is caused by the increase of fluid, significant flow speed, and heat transfer carried out through the boundary layer. As $R = 1.01$ (short dotted line) and $t = 30$ min, the change of interface is still insignificant. When time goes on to 360 min, the interface, which bends more, and greater fusion rate in the lower part of interface will be observed as the Darcy number gets larger. The above is due to heat transfer to the lower part of the interface as a result of the presence of only one counterclockwise eddy in the flow.

Figure 13 shows the change of average Nusselt number $\overline{Nu}$ on the hot side with respect to the Darcy number. We conclude from this figure that regardless of R (or T_h), the larger the Darcy number is, the larger $\overline{Nu}$ will be. Furthermore, as $R = 0.36$, maximum difference of $\overline{Nu}$ takes place for three different Darcy numbers, however, for $R = 0.53$, we have a minimum difference of $\overline{Nu}$. This can be understood in the following: at $R = 0.36$, the bigger the Darcy number is, the stronger the clockwise eddy is, which drops the temperature of the fluid near the hot side and increases the temperature gradient; for $R = 0.53$, the larger the Darcy number is, the stronger the two eddies on the left and right accordingly (Fig. 12). Since heat transfer still takes place indirectly, the flow near the hot side remains the higher average temperature. Viewing Fig. 11, we also find that the larger the Darcy number is, the bigger the change of $\overline{Nu}$ with respect to T_h (or R).

CONCLUSION

Summarizing the results of the numerical analysis, we have some important conclusions:

(1) The non-linear factor existing in the density-temperature relationship has a great influence on the temperature distribution, flow field, interface and heat transfer in the melting of ice in a porous media. As R becomes smaller and less than 0.5, the isothermal line distorts more, the clockwise eddy becomes bigger and stronger, and the upper interface bends to the right more than the lower part.

(2) When the Darcy number increases, we can get a better heat transfer, greater fusion rate of ice and greater distortion of interface.

(3) Heat transfer does not always increase with an increase of the hot side temperature. There exists a hot side temperature for minimum heat transfer.

(4) The heat transfer gets poorer on the hot side and better on the cold side as time goes on.

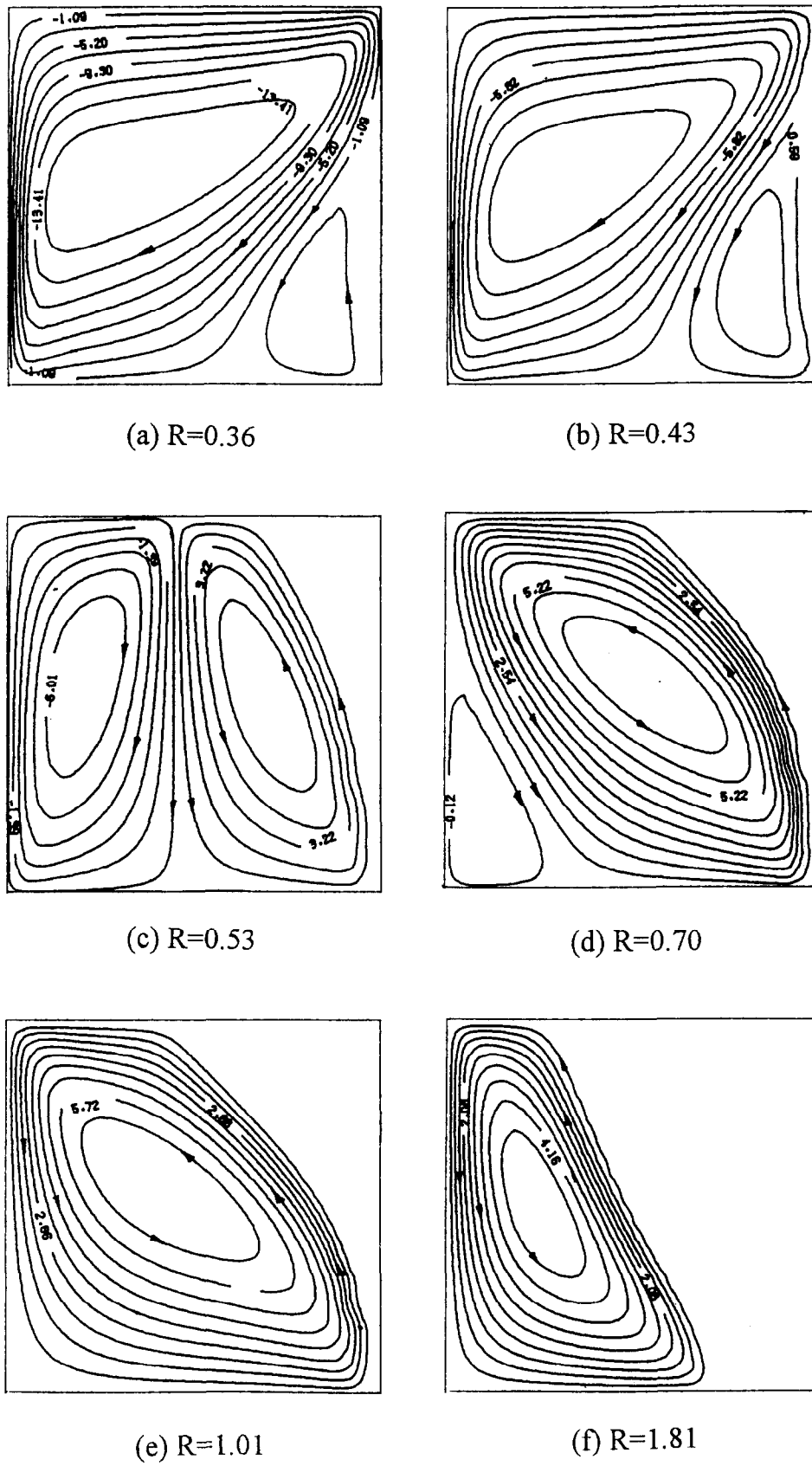

(a) R=0.36 (b) R=0.43

(c) R=0.53 (d) R=0.70

(e) R=1.01 (f) R=1.81

Fig. 9. The contour of the streamlines for different R values ($Da = 3 \times 10^{-5}$, $t = 600$ min).

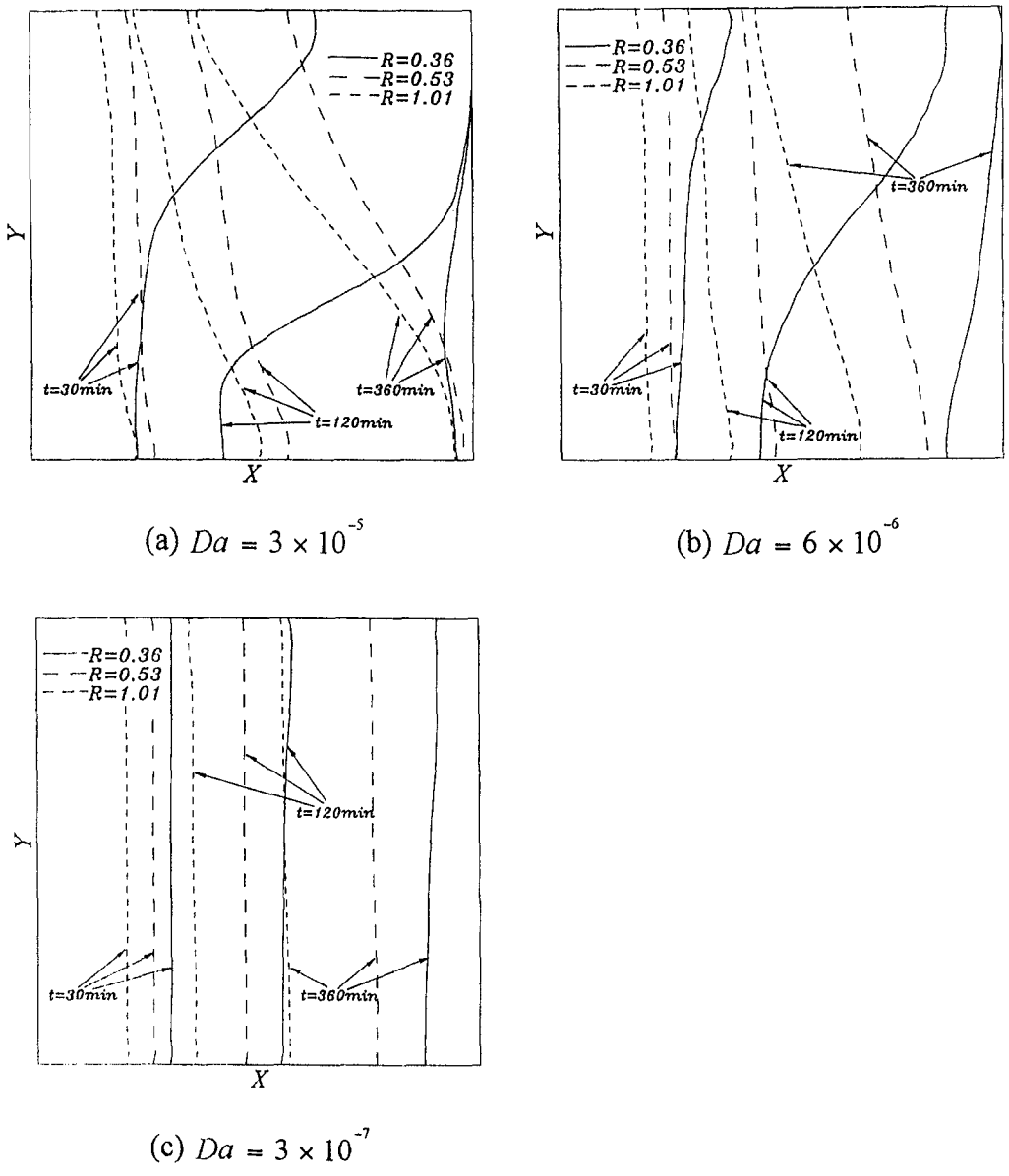

Fig. 10. The influence of maximum density parameter R on the interface positions.

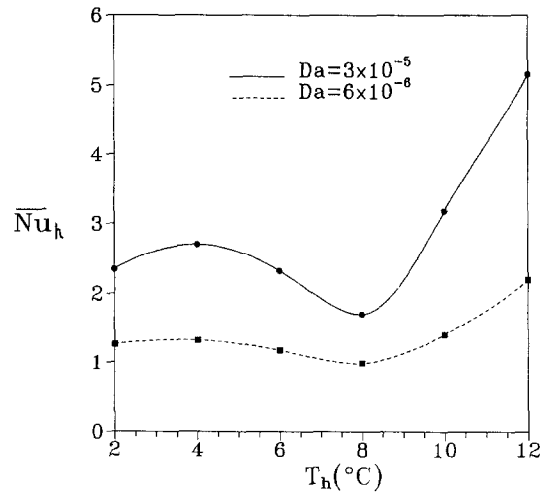

Fig. 11. The average Nusselt number at the hot side vs T_h at $t = 975$ min.

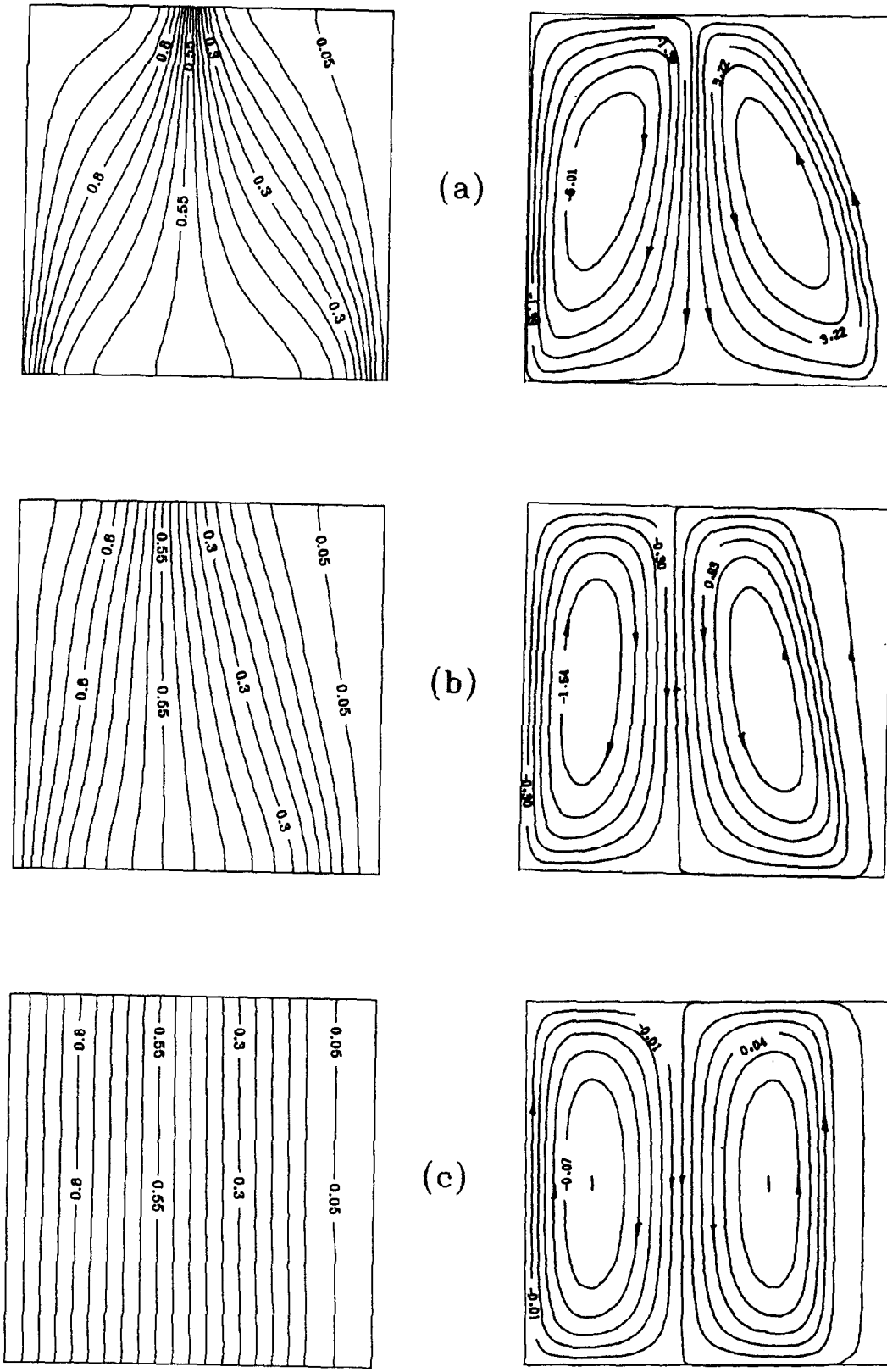

Fig. 12. The contours for $R = 0.53$ and $t = 600$ min streamlines at (a) $Da = 3 \times 10^{-5}$, (b) $Da = 6 \times 10^{-6}$, (c) $Da = 3 \times 10^{-7}$.

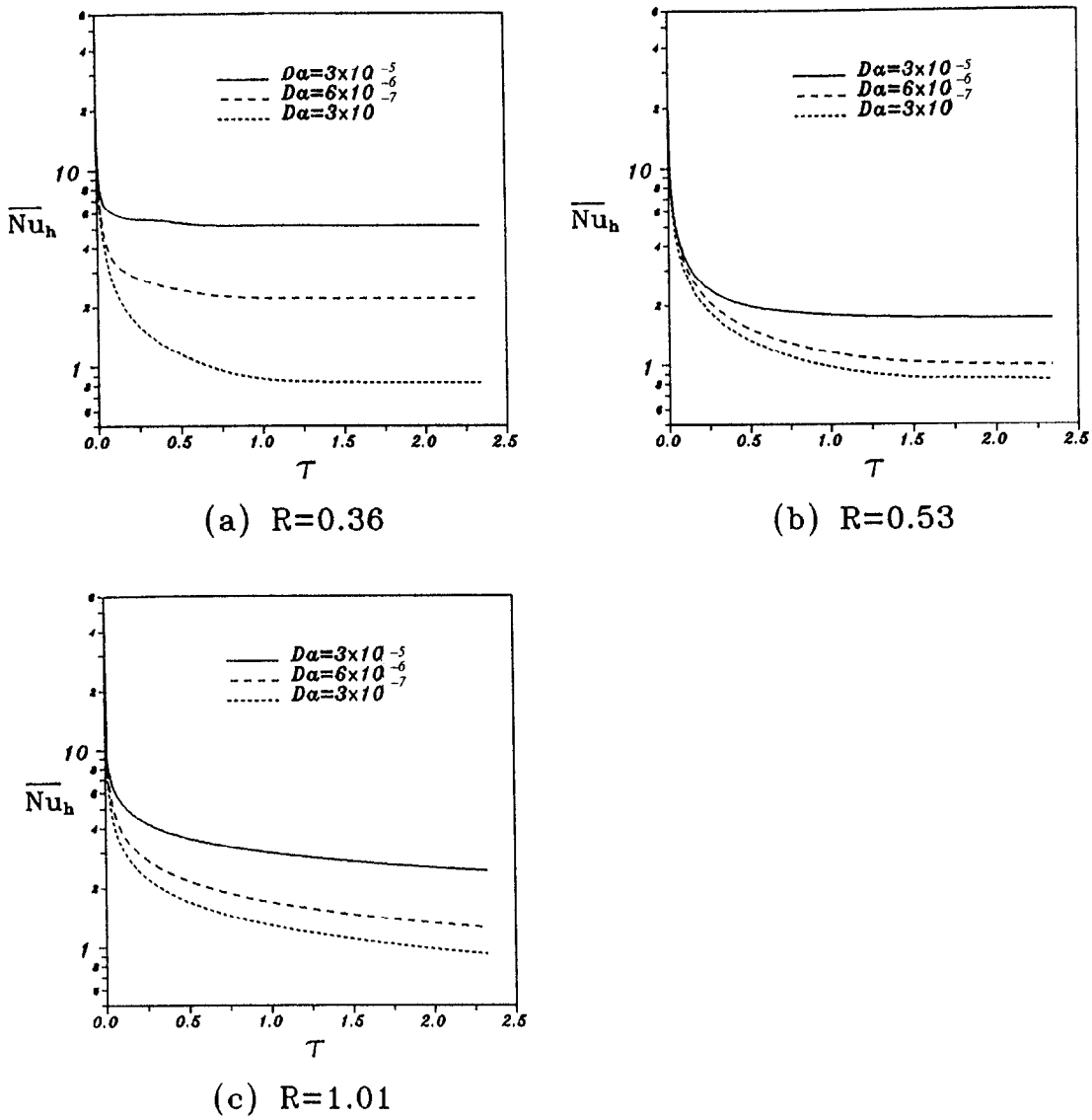

Fig. 13. The average Nusselt number at the hot side vs dimensionless time for different R and Da values.

REFERENCES

1. K. S. Udell, Heat transfer in porous media heated from above with evaporation, condensation and capillary effects, *ASME J. Heat Transfer* **105,** 485–492 (1983).
2. M. Kaviany, Boundary layer treatment of film condensation in the presence of a solid matrix, *Int. J. Heat Mass Transfer* **29,** 951–954 (1986).
3. M. Kazmierczak and D. Poulikakos, Melting from a flat plate embedded in a porous medium in the presence of steady natural convection, *Numer. Heat Transfer* **10,** 571–581 (1986).
4. X. Zhang, Natural convection and heat transfer in a vertical cavity filled with an ice-water saturated porous medium, *Int. J. Heat Mass Transfer* **36,** 2881–2890 (1993).
5. K. S. Chen and J. R. Ho, Effects of flow inertia on vertical, natural convection in saturated, porous media, *Int. J. Heat Mass Transfer* **29,** 753–759 (1986).
6. T. W. Tong and E. Subramanian, A boundary-layer analysis for natural convection in vertical porous enclosures use of the Brinkman-extended Darcy model, *Int. J. Heat Mass Transfer* **28,** 563–571 (1985).
7. K. Vafai and C. L. Tien, Boundary and inertia effects on flow and heat transfer in porous media, *Int. J. Heat Mass Transfer* **24,** 195–203 (1981).
8. C. Beckermann, S. Ramadhyani and R. Viskanta, Natural convection flow and heat transfer between a fluid layer and a porous layer inside a rectangular enclosure, *ASME J. Heat Transfer* **109,** 363–370 (1987).
9. C. Beckermann and R. Viskanta, Natural convection solid/liquid phase change in porous media, *Int. J. Heat Mass Transfer* **31,** 35–46 (1988).
10. B. Gebhart and J. Mollendorf, A new density relation for pure and saline water, *Deep-Sea Res.* **24,** 831–848 (1977).
11. D. S. Lin and M. W. Nansteel, Natural convection heat transfer in a square enclosure containing water near its

density maximum, *Int. J. Heat Mass Transfer* **30,** 2319–2329 (1987).
12. J. P. Van Doormaal and G. D. Raithby, Enhancement of the SIMPLE method for predicting incompressible fluid flows, *Numer. Heat Transfer* **7,** 147–163 (1984).
13. S. V. Patankar and D. B. Spalding, A calculation procedure for heat, mass and momentum transfer in three-dimensional parabolic flows, *J. Heat Mass Transfer* **15,** 1787–1806 (1972).
14. S. V. Patankar, *Numerical Heat Transfer and Fluid Flow*. Hemisphere Publishing, New York (1980).